Biophysical Chemistry, 35 (1990) 227–243
Elsevier

BIOCHE 01426

The interaction with DNA of unfused aromatic systems containing terminal piperazino substituents

Intercalation and groove-binding

W. David Wilson, Henryk J. Barton, Farial A. Tanious, Suk-Bin Kong and Lucjan Strekowski

Department of Chemistry and Laboratory for Microbial and Biochemical Sciences, Georgia State University, Atlanta, GA 30303, U.S.A.

Received 14 April 1989
Accepted 15 August 1989

Unfused aromatic system; Intercalation; DNA-drug interaction; Antitumor agent; Binding mechanism

A number of unfused tricyclic aromatic intercalators have shown excellent activity as amplifiers of the anticancer activity of the bleomycins and the 4′,6-diphenylpyrimidines, **2a** and **2b**, with terminal basic functions (4-methylpiperazino groups) have been synthesized to test the structural requirements for amplifier-DNA interactions. The terminal piperazine rings are bulky, have limited flexibility, and are twisted out of the phenyl ring plane in both **2a** and **2b**. With **2a** the pyrimidine is unsubstituted at position 5 and the conformation predicted by molecular mechanics calculations has a 25–30° twist between the phenyl and pyrimidine ring planes. With **2b** the 5-position is substituted with a methyl group and this causes a larger twist angle (50–60°) between the phenyl and pyrimidine planes. These conformational variations lead to markedly different DNA interactions for **2a** and **2b**. Absorption, CD and NMR spectral, viscometric, flow dichroism and kinetics results indicate that **2a** binds strongly to DNA by intercalation while **2b** binds more weakly in a groove complex. The general structure and conformation of **2a**, a slightly twisted, unfused-aromatic system with terminal piperazino groups is more similar to groove-binding agents such as Hoechst 33258 than to intercalators. The fact that **2a** forms a strong intercalation complex with DNA is unusual but in agreement with studies on other amplifiers of anticancer drug action. Molecular modeling studies provide a second unusual feature of the **2a** intercalation complex. While most well-characterized intercalators bind with their bulky and/or cationic substitutents in the DNA minor groove, the cationic piperazino groups of **2a** are too large to bind in the minor groove in an intercalation complex but can form strong interactions with DNA in the major groove. The tricyclic aromatic ring system of **2a** stacks well with adjacent base-pairs in the major-groove complex and the piperazino groups have good electrostatic and van der Waals interactions with the DNA backbone.

1. Introduction

A number of anticancer drugs bind strongly to DNA and this binding appears to be involved in at least one of the processes that leads to biological activity of the drugs [1–7]. The strong interactions have binding modes which fall into two categories: intercalation and specific interactions in the DNA grooves [1–10]. Intercalators typically have two to four fused ring aromatic systems which contain protonated nitrogens or have protonated side chains attached to the ring system [1–5]. Groove-binding agents are also aromatic cations but typically contain unfused aromatic systems with terminal basic functions [6,8,10]. The unfused aromatic system allows enough torsional freedom for the molecules to adopt a twist which closely matches the helical turn of the DNA grooves [10]. Based on these observations, it has generally been assumed that optimal interactions

Correspondence address: W.D. Wilson or L. Strekowski, Department of Chemistry, Georgia State University, Atlanta, GA 30303, U.S.A.

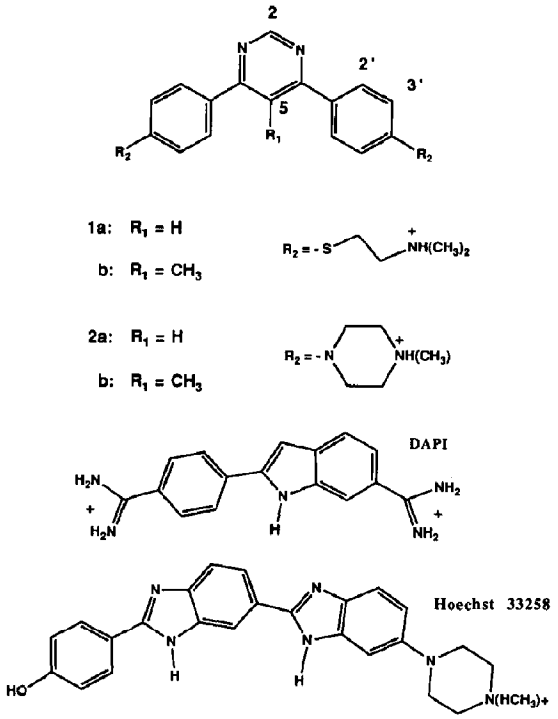

Fig. 1. Structures for **1a, 1b, 2a, 2b**, DAPI and Hoechst 33258. All compounds are shown as the predominant protonated species in solution at pH 7.

are obtained with fused ring systems for intercalation and unfused ring systems for groove complexes [8].

We have made two recent discoveries which extend the structural understanding of intercalation and groove-binding modes and which we believe are important for the design of DNA-interactive anticancer drugs and drug amplifiers. First, we have found a class of unfused aromatic cations which are structurally quite different from classical intercalators but which bind strongly to the DNA double helix by intercalation [11–14]. Compound **1a** (fig. 1), which has a twist of 20–25° between the phenyl and pyrimidine ring planes, is a typical example [11]. Its analogue, **1b** (fig. 1), which has a much larger intrinsic twist of 50–60° between the phenyl and pyrimidine ring planes due to the pyrimidine methyl substituent, binds more weakly to DNA and does not intercalate [11]. Second, we have found that classical groove-binding molecules such as 4′,6-diamidino-2-phenylindole (DAPI; fig. 1) can bind strongly to GC-rich and mixed AT/GC sequences in DNA by intercalation [15]. In a sequence of three to four AT-base-pairs DAPI has a very strong, specific-binding site in the DNA minor groove [16,17], the typical binding mode of groove-binding agents, but with DNA sequences containing GC base-pairs, intercalation is the preferred binding mode [15]. Multiple DNA-binding modes have also been observed with other drugs, such as phenosafranine, which has strong monomer-binding modes both by intercalation, with AT base-pair specificity, and by groove binding with GC specificity [2,18]. It is essential to elucidate these sequence- and ligand-dependent variations in DNA-binding mode in order to achieve a better understanding of the action of existing anticancer drugs and to design more rationally superior new drug candidates.

An additional promising development for potential enhancement of the activity of DNA-interactive anticancer drugs is indicated by the observation that some unfused aromatic cations can significantly enhance drug activity without a concomitant increase in toxicity [11–14,19,20]. The compounds alone need not possess anticancer activity and are thus termed amplifiers [20]. Amplification, for example, has been observed with the bleomycin family of metal-complexing glycopeptides, which have significant intrinsic clinical anticancer activity [13,14,19]. The most extensively studied member of this family is the bleomycin-Fe^{2+} complex, the activity of which is thought to be due to the interaction with and subsequent degradation of the DNA double helix in the presence of molecular oxygen [20–22]. The medicinal use of these compounds is, however, severely limited by toxic side effects. Amplifiers have the potential of significantly increasing the desired activity of bleomycin without a correlated increase in toxicity.

Although fused ring intercalators, such as ethidium, are weak amplifiers at low ratios of compound to DNA base-pairs, they become inhibitors of the bleomycin-induced degradation of DNA at high ratios [11–14]. Unfused aromatic cations which bind to DNA by intercalation show

good amplification at low ratios of amplifier to DNA base-pairs, and do not exhibit inhibition of the bleomycin-induced cleavage of DNA at very high ratios [11–14]. Compound **1a** (fig. 1) is one such unfused aromatic amplifier but the closely related analogue **1b**, which does not intercalate, is a very weak amplifier [11]. An additional unexpected feature of the **1a**-DNA intercalation complex is that the two cationic side chains of **1a** can fit easily into the DNA major groove but are sterically prevented from fitting into the minor groove [11]. Classical DNA intercalators such as ethidium, actinomycin and daunomycin intercalate with their bulky substituents and/or cationic groups in the DNA minor groove [1–7]. Bleomycin is also believed to bind to DNA from the minor groove [21,22] and competitive binding could explain the inhibition of bleomycin-induced chemistry at high concentrations of classical intercalators. In contrast, good amplifiers, such as **1a**, should bind to DNA from the major groove and would, thus, not compete with bleomycin for binding to DNA even at high ratios.

To test these ideas and to design new and potentially superior DNA interactive anticancer drugs and drug amplifiers, it is extremely important to develop criteria for the selective intercalation of aromatic molecules from the major groove of the DNA double helix. As part of this effort, we report here the synthesis and DNA-interaction properties of unfused aromatic cations **2a** and **2b** (fig. 1). Compounds **2a** and **2b** are similar to **1a** and **1b**, respectively, in torsional angles for the phenyl-pyrimidine ring planes but the cationic piperazine rings of **2a** and **2b** are larger and more rigid than the alkylamino cationic groups of **1a** and **1b**. As can be seen by comparing the structures in fig. 1, **2a** more closely resembles the well-characterized groove-binding molecule Hoechst 33258 [6,23,24], than the classical fused ring intercalators [1–5,7,8]. It has been clearly established that Hoechst 33258 has a very high specificity for binding in the minor groove and that the piperazine ring of Hoechst can be accommodated in the narrow groove of DNA [6,23,24]. The experiments reported here were designed to determine whether compounds such as **2a** and **2b** bind by intercalation or via groove-interaction modes, whether the piperazino groups are in the minor or major groove in the DNA complex, and to provide a molecular model for these complexes.

2. Experimental

2.1. Synthesis of 2a and 2b

2.1.1. 4,6-Bis[4′-(4″-methylpiperazino)phenyl]pyrimidine (2a)

Compound **2a** was prepared according to scheme 1. A solution of 1-(4′-aminophenyl)-4-methylpiperazine (**4**) [25] in aqueous HBr was treated with $NaNO_2$, and the resultant diazonium salt was reacted with CuBr using a general procedure [26] to give 1-(4′-bromophenyl)-4-methylpiperazine (**5**). Compound **5** was purified by chromatography on silica gel eluting with triethylamine/hexanes (1 : 9) followed by crystallization from hexanes: yield 40%; m.p. 72–74°C; ^{1}H-NMR (C^2HCl_3) δ (ppm), 2.31 (s, 3H), 2.51 (t, $J = 5$ Hz, 4H), 3.14 (t, $J = 5$ Hz, 4H), 6.72 (d, $J = 9$ Hz, 2H), 7.27 (d, $J = 9$ Hz, 2H). A solution of **5** (0.84 g, 3.3 mmol) and *N,N,N′,N′*-tetramethylethylenediamine (0.5 ml) in diethyl either (35 ml) was treated at −30°C with *n*-butyllithium (2.6 M in hexanes, 1.3 ml, 3.4 mmol), and the mixture was allowed to react at 0°C for 30 min. The resultant lithium reagent, **6**, was treated with a solution of pyrimidine (0.39 g, 5 mmol) in diethyl ether (5 ml), and the mixture was worked up using our general procedure described previously [19,27] to give 1-methyl-4-[4′-(4″-pyrimidinyl) phenyl]piperazine (**7a**). Crude compound **7a** was

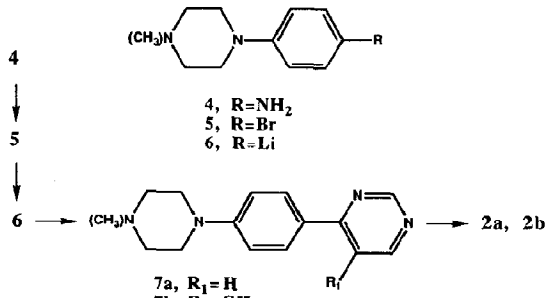

Scheme 1.

purified by chromatography on silica gel with triethylamine/hexanes (2:8) as an eluent followed by crystallization from toluene to give 0.35 g (57%): m.p. 158–160°C; ^{1}H-NMR (C^2HCl_3) δ (ppm), 2.40 (s, 3H), 2.60 (t, $J = 5$ Hz, 4H), 3.40 (t, $J = 5$ Hz, 4H), 6.96 (d, $J = 9$ Hz, 2H), 7.51 (d, $J = 6$ Hz, 1H), 8.00 (d, $J = 9$ Hz, 2H), 8.65 (d, $J = 6$ Hz, 1H), 9.15 (s, 1H). The subsequent reaction of **7a** with **6** using the same procedure and workup [19,27] gave compound **2a**, which was purified by chromatography on silica gel with dichloromethane/ triethylamine/ethanol (1:1:1) as an eluent. Compound **2a** was treated with HBr [11] and the resultant salt was crystallized twice from 95% ethanol; yield 36% of **2a** · 3HBr · H_2O; m.p. 310–315°C. Satisfactory microanalyses (C, ±0.3%; H, ±0.1%0 were obtained for **2a** ($C_{26}H_{32}N_6 \cdot 3HBr \cdot H_2O$) and the intermediate products **5** ($C_{11}H_{15}BrN_2$) and **7a** ($C_{15}H_{18}N_4$).

2.1.2. *5-Methyl-4,6-bis[4′-(4″-methylpiperazino) phenyl]pyrimidine (2b)*

Substitution of 5-methylpyrimidine for pyrimidine in the reaction with lithium reagent **6** described above and then followed by the same workup gave 1-methyl-4-[4′-(5″-methyl-4″pyrimidinyl)phenyl]piperazine (**7b**): yield 56%; m.p. 106–107°C; ^{1}H-NMR (C^2HCl_3) δ(ppm), 2.33 (s, 3H), 2.42 (s, 3H), 2.52 (t, $J = 5$ Hz, 4H), 3.31 (t, $J = 5$ Hz, 4H), 6.96 (d, $J = 9$ Hz, 2H), 7.60 (d, $J = 9$ Hz, 2H), 8.47 (s, 1H), 9.02 (s, 1H). Compound **7b** was reacted with lithium reagent **6** using the procedure described above, and the resultant product **2b** was transformed into a salt **2b** · 3HBr · H_2O: yield 30%; m.p. 261–264°C. Satisfactory microanalyses (C, ±0.3%; H, ±0.1%) were obtained for **2b** ($C_{27}H_{34}N_6 \cdot 3HBr \cdot H_2O$) and **7b** ($C_{16}H_{20}N_4$).

2.2. *Buffers*

Pipes buffers contained 10 mM Pipes, 1 mM EDTA, and NaCl as follows: Pipes 00, no added NaCl; Pipes 10, 0.1 M NaCl; Pipes 20, 02 M NaCl; Pipes 30, 0.3 M NaCl; Pipes 50, 0.5 M NaCl. All were adjusted to pH 7.0.

2.3. *DNA samples*

Calf thymus DNA from Worthington and polymers from P-L Biochemicals were prepared as previously described [28,29].

2.4. *Viscosity assay*

Viscometric measurements were made in Cannon-Ubbelhode semimicro-dilution viscometers as previously described [30]. Sonicated calf thymus DNA (~ 600–800 bp in length) in Pipes 00 buffer at concentrations of approx. 1×10^{-4} M was used for measuring viscosity increases in linear DNA with increasing drug concentrations.

2.5. *Spectrophotometric binding*

Absorbance measurements were made on a Cary 219 spectrophotometer interfaced to an Apple IIe microcomputer through a bidirectional digital communications port. Cell holders were thermostatted by using Haake circulating water baths. To remove some of the random error, for each absorbance measurement the microcomputer calculated the average of 100 acquired absorbance readings at a preselected wavelength for the compound under study. These averaged absorbance values were converted by the microcomputer to ν (mol compound bound/mol DNA base-pairs) and free ligand concentrations using the free and bound extinction coefficients for the compound. At the end of the titration, the computer constructed Scatchard plots for the digitized data which were in the fraction bound range, 0.2–0.8 [28,29]. Any binding results outside of this range are subject to large systematic errors due to experimental inaccuracies in extinction coefficients. The computer then calculated nonlinear least-square best-fit K (equilibrium constant) and n (base-pairs per binding site) values from the site-exclusion method of McGhee and Von Hippel [31].

2.6. *NMR*

The spectra of solutions of **2a** or **2b** were obtained as previously described [11,12,29] in ^2H_2O buffer (0.01 M phosphate, 0.001 M EDTA, 0.1 M

NaCl, pH 7) at high temperature (50–80° C) and low enough concentration (0.5 mM or less) so that no concentration-induced shifts were observed. Highly sonicated DNA samples (~ 200 bp) were then added and the shifts observed. NMR spectra were collected on a Varian VXR 400 spectrometer at a spectral width of 4500 Hz, with 10000 data points, a 1s relaxation delay, typically 128 transients and 3-(trimethylsilyl)propionic acid (TSP) as an internal reference.

2.7. Flow dichroism

Flow dichroism instrumentation was as previously described [32] with a rectangular (0.025 × 1 × 3 cm) quartz cell. Solutions were prepared with gentle stirring by adding ligand solutions to an unsonicated CT DNA (7.5 mM) solution. Data were obtained by recording the relative absorbance before, during, and after flow. Only the results in which absorbance was the same before and after the flow were used in the calculations. The linear dichroism, D, was calculated as the difference $(A_{\parallel} - A_{\perp})$ at 260 nm or at the long-wavelength maximum of the complex. To determine the absorbance of the DNA solutions without flow (A_0), an aliquot of solution was added to the low-salt Pipes 00 buffer which was used to ensure minimal dissociation of the ligand from the DNA. The reduced dichroism (^{red}D) was determined as $(A_{\parallel} - A_{\perp})/A_0$.

2.8. Stopped-flow kinetics

Kinetics measurements were made with a Hi-Tech SF-51 stopped-flow spectrometer and the software provided with the instrument was used for both data acquisition and analysis. First-order kinetics results can be fitted with a nonlinear least-squares routine which allows the determination of up to three amplitudes and rate constants for first-order exponential decays. The fitting routine is based on the Marquardt gradient-expansion method. The data acquisition is carried out via a high-speed (> 80 kHz) 12 bit analogue-to-digital convertor with an HP-330 computer interfaced to SF-51. Single-wavelength kinetic records of voltage vs. time were collected and converted to absorbance. Typically five to eight runs were collected and averaged by the computer to improve the signal-to-noise ratio. Dissociation reactions were monitored by mixing equal volumes (100 μl) of a DNA-drug complex with a 1% solution of SDS at the same ionic strength. The temperature control was through a Haake A81 refrigerated water bath. The measurements were made in a 1 cm path length quartz cell at the desired wavelength and temperature.

2.9. Circular dichroism

CD spectra were obtained on a Jasco J-600 spectrometer interfaced to an IBM-PC computer. The software supplied by Jasco provided instrument control, data acquisition and manipulation. Typically solutions of compound in Pipes 00 buffer at 25° C were scanned from 450 to 300 nm in a 5 cm quartz cuvette. Concentrated solutions of DNA were added and the sample rescanned at all desired ratios.

2.10. Molecular modeling

Atom point charges were calculated for **1a**, **1b** and **2a**, **2b** using the AMPAC program package from the Quantum Chemistry Program Exchange. Molecular Mechanics calculations were conducted with the AMBER Force Field in the program MACROMODEL from Professor Clark Still of Columbia University as previously described [12,15]. The compounds were docked with a standard B-form DNA generated in MACROMODEL using Arnott coordinates or into an intercalation site in B-form DNA (to be described elsewhere).

3. Results

3.1. Structures of 2a and 2b

We have determined optimized structures for **2a** and **2b** with the AMBER force field in the MACROMODEL molecular-mechanics program (fig. 2). The phenyl-pyrimidine ring plane torsional angles are 25–30° for **2a** and 50–60° for **2b**. As expected, these values are essentially the same as those observed for the similarly sub-

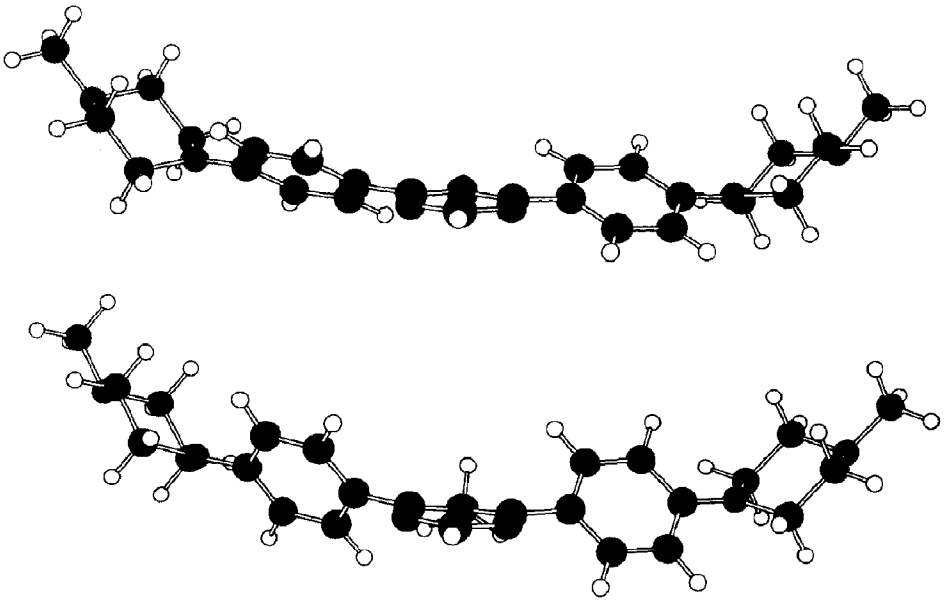

Fig. 2. Molecular mechanics minimized conformations for **2a** (top) and **2b** (bottom): carbon atoms are represented by dark shading nitrogens by light shading and hydrogens by no shading. The view into the central pyrimidine ring is the same for both compounds so the larger twist of the phenyl-pyrimidine-phenyl aromatic system in **2b** can easily be seen.

stituted **1a** and **1b** when using the AMBER force field [11,12]. The barrier to a planar three-ring aromatic system for **1a** and **2a** is approx. 4 kJ/mol while that for **1b** and **2b** is approx. 33 kJ/mol.

Because of steric hindrance, the cationic piperazine rings of **2a** and **2b** are rotated away from the ring planes of the attached phenyl rings (fig. 2) and have much less torsional freedom than the alkylamino side chains of **1a** and **1b**. The comparison of **2a** to Hoechst 33258 is interesting (fig. 1). Calculations with MACROMODEL suggest that two benzimidazole rings of Hoechst are in approximately the same plane while the *N*-methylpiperazino group as with **2a**, **2b** is twisted significantly out of the aromatic plane. The structure of Hoechst 33258 is, thus, quite simlar to that of **2a**.

3.2. Evaluation of binding mode

Viscometric titrations of DNA with ligands, flow dichroism of DNA complexes, NMR titrations of ligands with DNA, and DNA-complex

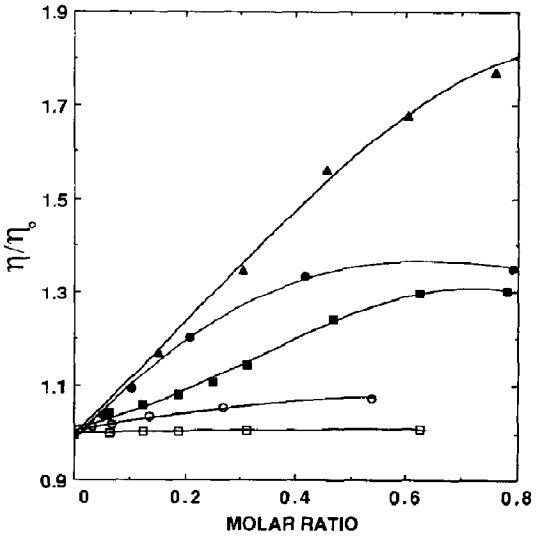

Fig. 3. Viscometric titrations of calf thymus DNA with ethidium (▲), **1a** (■), **1b** (□), **2a** (●), and **2b** (○). Titrations were performed in Pipes 00 buffer at 31°C with sonicated DNA of 600–800 bp average length. The reduced specific viscosity ratio is plotted vs. the molar ratio of compound to DNA base-pairs. Results for **1a** and **1b**, from ref. 11, are included for comparison.

Table 1

The reduced dichroism (^{red}D) for calf-thymus DNA complexes [a]

Compound	^{red}D (260 nm)	Complex maximum wavelength (nm)	^{red}D
Calf thymus DNA	−0.15	–	–
1a	−0.15	330	−0.061
1b	−0.13	305	+0.002
2a	−0.16	370	−0.052
2b	−0.15	340	+0.004
Hoechst 33258	−0.13	347	+0.078
Propidium	−0.14	520	−0.170

[a] Flow dichroism results (^{red}D) are given at the DNA maximum wavelength (260 nm) and at the bound ligand maximum wavelength in Pipes 20 buffer.

dissociation kinetics studies as a function of salt concentration were conducted with **2a** and **2b** to evaluate their DNA-binding mode.

3.3. Viscometric titrations

Viscosity changes for calf thymus DNA are plotted in Fig. 3 as a function of the molar ratio of compound to DNA base-pairs. As can be seen, the viscosity increase in DNA induced by binding of both **1a** and **2a** is similar but less than that observed with ethidium. Compound **1b** gives very small viscosity increases and the changes induced by **2b** are slightly larger.

3.4. Flow dichroism

Dichroism comparisons in a flow system were conducted both at 260 nm and at the maximum wavelength of the complex above 300 nm for several dicationic compounds: the intercalator propidium; the groove-binding molecule Hoechst 33258; and **1a**, **1b**, **2a** and **2b** (table 1). As expected from their binding modes [8], the propidium-DNA complex has large negative dichroism values at both 260 nm and the compound maximum wavelength in the complex, while the Hoechst complex has a negative dichroism at 260 nm and a positive dichroism at the long-wavelength maximum characteristic of the bound molecule. Compounds **1a** and **2a** exhibit similar negative reduced dichroism values at the compound maximum wavelength which are less than the values observed for DNA base-pair and for propidium. Neither **1b** nor **2b** exhibits significant dichroism values at the compound maximum wavelength although results with both show a small systematic trend in the positive direction (table 1).

3.5. Aromatic proton NMR shifts

The aromatic protons of intercalators shift upfield by 0.4–1.0 ppm as the compounds bind to DNA and are influenced by the local anisotropic shielding effects of the DNA base-pairs [34]. Compounds which bind in the DNA grooves generally display much smaller induced shifts which may be either upfield or downfield. As with **1a** [11], addition of calf thymus DNA to **2a** results in line broadening and upfield shifts for the **2a** aromatic protons (table 2). As with **1b** [11], **2b** displays much sharper lines when bound to DNA and has only very small induced shifts of its proton signals on binding to DNA (table 2). We conducted these experiments at high temperature (~ 10–15 °C below the DNA T_m) to obtain line sharpening due to molecular motion and fast exchange of the bound molecule among states. Slow exchange can be obtained at low temperature but the spectral lines of the bound ligand are too broad to follow in a titration with DNA.

Calf thymus DNA signals show considerable chemical shift dispersion and all of its proton

Table 2

Chemical shifts for aromatic protons of **1a**, **1b** and **2a**, **2b** (δ) and chemical shift changes on addition of excess calf thymus DNA ($\Delta\delta$)

Compound		H2	H5	H2′, H6′	H3′, H5′
1a	δ	9.16	8.25	8.08	7.64
	$\Delta\delta$	−0.51	−0.48	−0.41	−0.41
2a	δ	9.08	8.22	8.13	7.27
	$\Delta\delta$	−0.41	−0.40	−0.37	−0.30
1b	δ	9.03	–	7.66	7.66
	$\Delta\delta$	−0.06		−0.04	−0.04
2b	δ	8.97	–	7.67	7.26
	$\Delta\delta$	−0.07		−0.03	−0.06

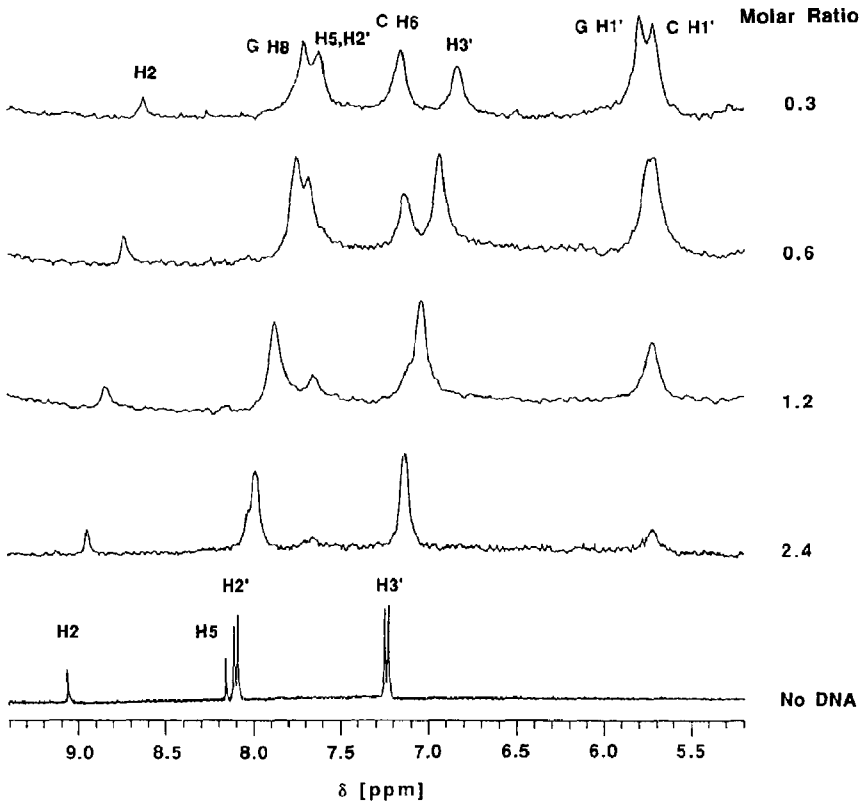

Fig. 4. The sugar H1′ and aromatic proton region for an NMR titration of **2a** with poly[d(G − C)$_2$] at 80 °C. Aromatic proton assignments (see fig. 1 for numbering) are shown on the top and bottom spectra. The molar ratio of compounds/DNA base-pairs is indicated at the right of each spectrum.

signals are broadened almost to baseline below the T_m. With DNA polymers, however, the signals are intrinsically sharper and signals for both ligand and polymer can be seen. The titration of **2a** with sonicated poly(G-C)$_2$ is shown in fig. 4 as an example. As the ratio of DNA to compound is increased, the aromatic signals of **2a** shift significantly upfield and broaden. At the high temperature of the experiment, free and bound **2a** are in fast exchange and the signals shift as a single band. The G-H8 and C-H6 signals can also be seen in this experiment and, as the ratio of **2a** to DNA increases, the signals shift slightly upfield, indicating that the aromatic ring-current induced shifts due to bound **2a** are larger than the base-pair effects in the uncomplexed duplex. The sugar H1′ protons for G H1′ and C H1′ are resolved in the uncomplexed duplexed but as **2a** is added to the DNA, the G H1′ signal moves significantly upfield and the two signals merge (fig. 4).

Both **2a** and **2b** were obtained and purified by crystallization as *stable* trihydrobromide salts. The most probable cationic sites of these salts in the solid state are two terminal N-CH_3 and the central pyrimidine moieties. In contrast, only the terminal amino groups of the analogues **1a** and **1b** are protonated in crystals, H_2O solutions, and the complexes with DNA [11]. Comparison of the ^{1}H-NMR spectra of **1a** and **2a** taken in ^2H_2O revealed closely similar chemical shifts for the respective C2-proton of the pyrimidine ring (table 2). The same result was obtained for the methyl analogues **1b** and **2b** and for the two pairs of compounds in complexes with DNA. It must be

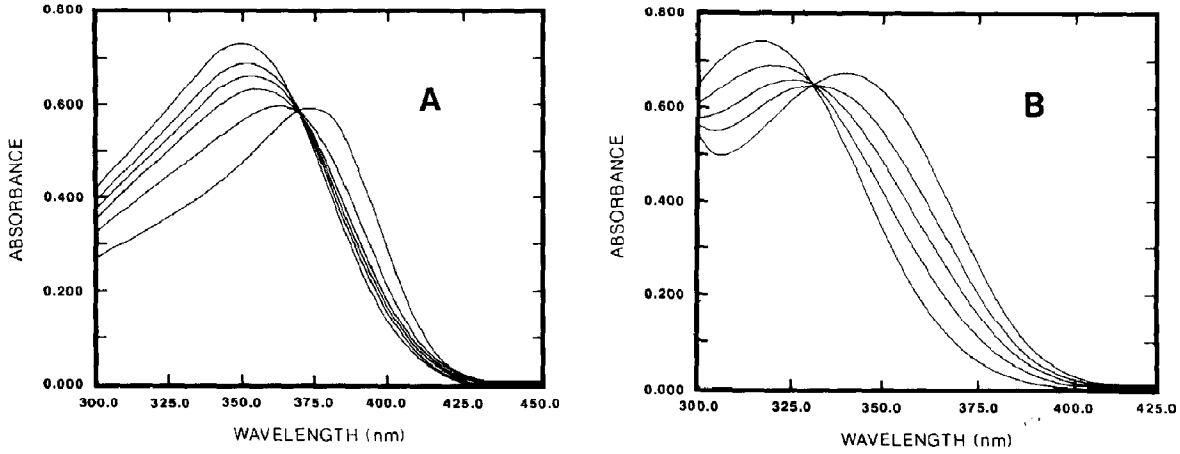

Fig. 5. Spectrophotometric titrations of **2a** (A) and **2b** (B) with calf thymus DNA. [**2a**] 1.3×10^{-5} M; [**2b**] 1.7×10^{-5} M. Free compound spectra have the highest absorbance. Shifts to longer wavelength and hypochromic changes occur on addition of DNA. Titrations were conducted in Pipes 00 buffer at 25° C in 1 cm path length cuvettes. DNA was added to a 10-fold excess of base-pairs to compound and little spectral change occurred after that ratio at the low salt concentration for this experiment.

concluded, therefore, that (i) compounds **2a** and **2b** are dicationic both free in solution and complexed with DNA, and (ii) the formation of solid trihydrobromide salts of **2a** and **2b** is due to favorable packing forces for the tricationic species in crystals.

3.6. Visible absorption spectral shifts

DNA-induced spectral shifts, above 300 nm where absorption from DNA does not overlap, can be used to monitor ligand-binding strengths and rates [28]. Spectra for **2a** and **2b** are shown in fig. 5, both in the free state and in the presence of increasing amounts of DNA. Isosbestic points are obtained in both titrations. Compound **2a** has a maximum at 345 nm (extinction coefficient, $E = 29\,500\ M^{-1}\,cm^{-1}$) in the free state and this shifts to approx. 370 nm when bound to DNA (fig. 5A). Compound **2b** has a maximum at a lower wavelength with a lower extinction coefficient (315 nm, $E = 23\,000\ M^{-1}\,cm^{-1}$). The maximum shifts to approx. 340 nm for the compound complexed with DNA (fig. 5B). Thus, in spite of dramatic structural differences in these two compounds and their varying effects on the physical properties of DNA, very similar spectral shifts to longer wavelength are induced for both compounds on binding to the double helix. Similar effects have been observed with **1a** and **1b** [11]. All compounds obeyed Beer's law at concentration below 10^{-4} M.

3.7. Dissociation kinetics

Spectral changes, as shown in fig. 5, can also be used to monitor the kinetics of the interaction of compounds with DNA [28,33]. The association of **1a**, **1b**, **2a** and **2b** and the dissociation of bound **1b** and **2b** are too fast to measure by stopped-flow techniques. The dissociation kinetics of **2a**- and **1a**-DNA complexes can be measured under reasonable conditions and a typical SDS-driven dissociation curve for a **2a**-DNA complex is shown in fig. 6 along with a two-exponential fit to the results. A single-exponential curve does not give a satisfactory fit to the data, a three-exponential curve does not significantly improve the root-mean-square deviation or the residual plot for the fit, and both were thus rejected [33]. Dissociation results for the calf thymus DNA complex of **1a** also required a two-exponential fit and results for **1a** and **2a** are given at 25° C in table 4. Similar experiments on a **2a** complex with poly[d(A − T)$_2$] also required a two-exponential fit but results with poly[d(G − C)$_2$] could be fitted with a single-exponential curve (table 4).

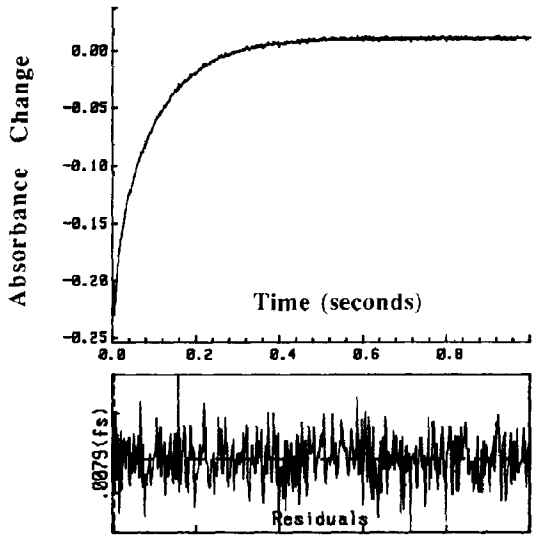

Fig. 6. A stopped-flow kinetics trace of the absorbance change vs. time for the SDS-driven dissociation of a **2a**-calf thymus DNA complex. The experiment was conducted in PIPES 00 buffer at 25°C by mixing 100 μl of a **2a**-DNA complex with 100 μl of a 1% SDS solution in buffer. [**2a**] 2×10^{-5} M; ratio 0.1 **2a**/base-pair. The results were fitted to a two-exponential curve and a plot of the residuals is shown at the bottom.

Kinetics experiments were also conducted with the complexes of **2a** with calf thymus DNA, poly[d(G − C)$_2$] and poly[d(A − T)$_2$], as a function of salt concentration to evaluate the binding mode at quite different DNA sequences [28,33]. The slope of log k_d vs. log[Na^+] plots for all complexes at several temperatures is 0.6 ± 0.1 as expected for an intercalation binding mode [28,33,35]. The k_d values for the two polymer complexes were also determined over the temperature range 15–45°C and yielded enthalpies of activation of 77 kJ/mol for the AT complex and 89 kJ/mol for the GC complex (table 4). Although this suggests that a higher enthalpy of activation may partially account for the slower dissociation of **2a** from poly[d(G − C)$_2$], the experimental error range of ±5 kJ/mol, due to the very fast rates at high temperatures, precludes definitive resolution of this question.

Table 4
Kinetic data for SDS-driven dissociation of **1a**- and **2a**-DNA complexes [a]

Compound	DNA	k_1 (s^{-1})	k_2 (s^{-1})	A_1/A_2	ΔH_{act} (kJ/mol)
1a	calf thymus DNA	246	68	1.6	–
2a	calf thymus DNA	39.3	11.5	0.22	90.4
2a	Poly[d(G−C)$_2$]	14.3	–	1	89.1
2a	Poly[d(A−T)$_2$]	180	41.7	0.39	77.4

[a] Temperature of 25°C and total sodium concentration of 0.036 M after mixing. Rate constants in the two-exponential fits are indicated by k_1 and k_2 with amplitude ratio A_1/A_2. ΔH_{act} denotes the activation enthalpy for dissociation.

Table 3
Binding constants of **2a** and **2b** with different DNA samples [a]

DNA	$K(\times10^{-3})$	
	2a	**2b**
Calf thymus	900	130
Poly[(dA−dT)$_2$]	2500	500
Poly[(dG−dC)$_2$]	520	60

[a] In Pipes 00 buffer at 25°C. The numbers of apparent base-pairs per binding site, n, in the McGhee-von Hippel model are 2.5–3 for these compounds.

3.8. Spectrophotometric binding constants (K)

Spectral shifts of the type shown in fig. 5 can be used under appropriate conditions (section 2.5) to determine K (table 3) for the interaction of **2a** and **2b** with DNA [28]. Under a standard set of conditions, the following observations were made: K for **2a** is greater than for **2b** by a factor of approx. 8 with calf thymus DNA. K for **2a** is greater than for **1a** by a factor of approx. 2 and K for **2b** is greater than for **1b** by a factor of approx. 5. Both **2a** and **2b** show a slight AT specificity; the K values for poly[d(A − T)$_2$] are approx. 5-times greater than for poly[d(G − C)$_2$].

The comparative K values for **2a**, **2b** and **1a** with calf thymus DNA are presented more quantitatively in fig. 7 as log K vs. −log[Na^+] plots. The binding of **1b** is too weak to determine accurately at salt concentrations above 0.050 M and is shown only at low salt concentration. The slopes for the other three compounds are 2.0 ± 0.1, indicating that all three molecules form two ion pairs with phosphate groups in their DNA complexes [28,35].

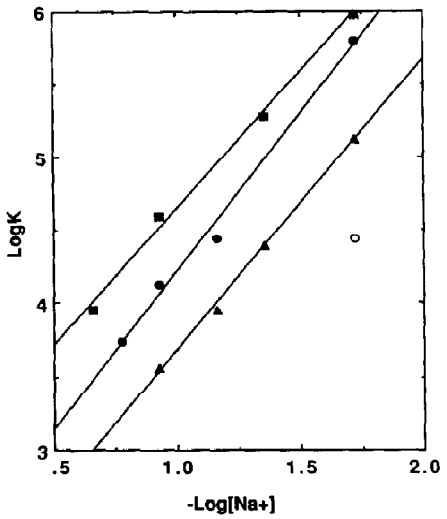

Fig. 7. Plots of log K vs. $-\log [Na^+]$ for **1a** (●), **1b** (○), **2a** (■), **2b** (▲). Results for **1a** and **1b** are from ref. 11 and are included for comparison. The solid lines are linear least-squares best-fit values to the data.

3.9. Circular dichroism

Compounds **1a**, **1b** and **2a**, **2b** have no intrinsic CD but have induced CD spectra on binding to DNA (fig. 8). All complexes have positive induced CD at the wavelength of maximum absorbance. Although the four spectra are somewhat similar, they show significant differences which agree with different binding modes for the -H relative to the $-CH_3$ substituted compounds. The maximum induced CD, for example, is greater for **1b** than **1a** and for **2b** vs. **2a**. Both **1a** and **2a** complexes have negative induced CD bands between 300 and 350 nm but **1b** and **2b** do not (fig. 8A). Although these CD spectra do not specify the type of DNA complex conformation, they clearly illustrate that **1a** and **2a** complexes fall into a similar conformational class which is different from that for **1b** and **2b** complexes.

The induced CD of **2a** was also investigated in complexes with both poly[d(G − C)$_2$] and poly[d(A − T)$_2$] (fig. 8B). The CD spectrum of **2a** with poly[d(A − T)$_2$] is similar to that observed with calf thymus DNA and has a large positive CD band between 350 and 400 nm and a smaller negative band between 300 and 350 nm. The intensities of both the positive and negative bands are, however, larger with poly[d(A − T)$_2$] than with calf thymus DNA. With poly[d(G − C)$_2$] the intensity of the 350–400 nm band is significantly less than with calf thymus DNA and a minimum, but no negative band, is observed between 300 and 350 nm (fig. 8B).

3.10. Molecular modeling

Docking experiments were performed with **2a** and a standard intercalation site at the central CG in the DNA sequence d(CGTACGTACG). There are three possible types of intercalation complexes with the phenyl-pyrimidine-phenyl ring system of **2a**: (1) a threading type of complex with one piperazine ring in each of the DNA grooves; (2) a complex with both piperazine rings in the minor groove; and (3) a complex with both piperazino groups in the major groove [11]. The half-life for dissociation of **2a** from DNA is approx. 100 ms at 25 °C (section 3.7) and this is too fast to allow the base-pairs to open to an extent sufficient to allow one of the bulky, cationic piperazino groups to slide through in the threading model. This type of complex can, thus, be rejected. In the minor-groove complex there are several close contacts between the piperazino groups and the DNA backbone residues. There are no intercalation geometries which do not have close contacts and during molecular mechanics minimization, **2a** is forced out of the intercalation site to relieve the unfavorable steric clash at the DNA backbone. The minor-groove model is, thus, also rejected.

As found previously with **1a** [11], a quite acceptable intercalation complex of **2a** with the side chains in the major groove can be constructed (fig. 9). The piperazino groups in the major groove do not have unfavorable steric clash with DNA atoms and have favorable van der Waals and electrostatic interactions with DNA. Due to the rigidity and size of the piperazino groups, there is little flexibility in positioning **2a** in the intercalation site shown in fig. 9A. Overlap of the aromatic system of **2a** with DNA base-pairs at the intercalation site can be seen in the view parallel to the helix axis (fig. 9B).

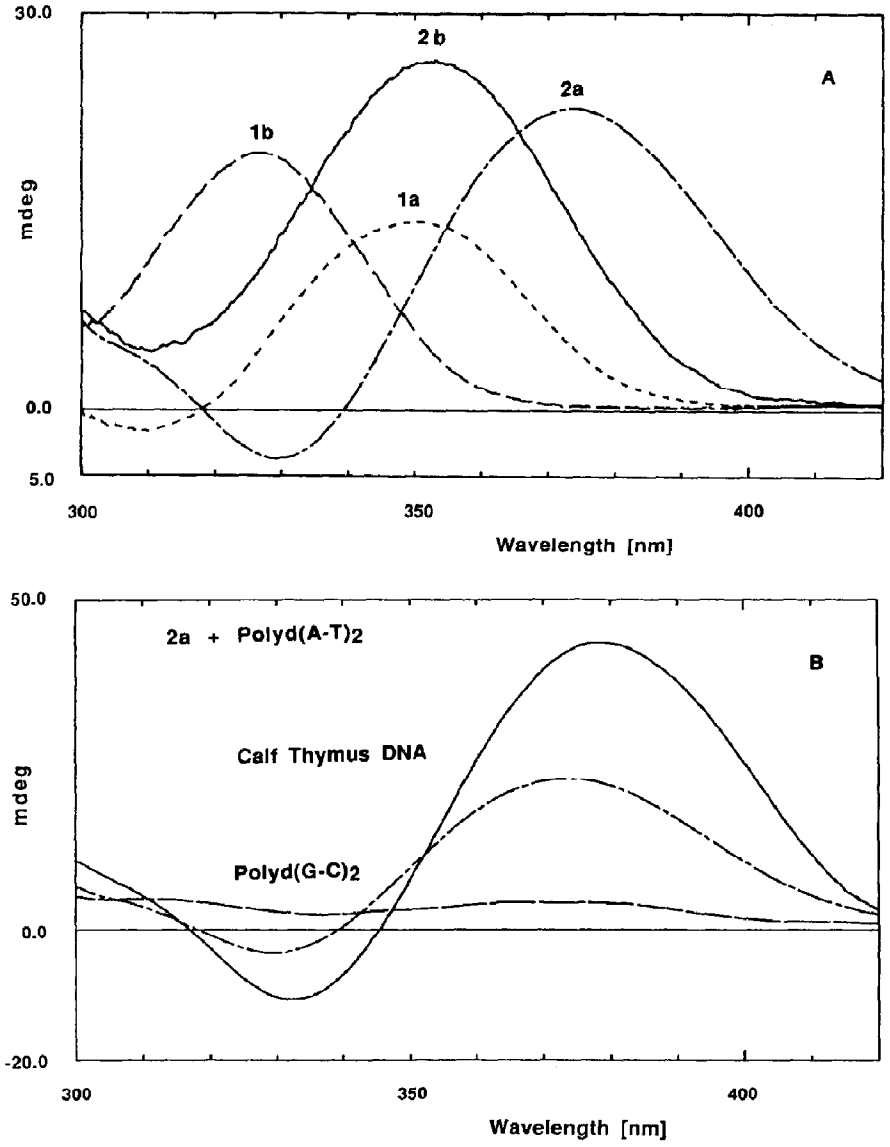

Fig. 8. (A) Circular dichroism spectra for **1a** (----), **1b** (— —), **2a** (— — —) and **2b** (———) with calf thymus DNA and (B) for **2a** with poly [d(A – T)$_2$] (———), calf thymus DNA (— - —) and poly [d(G – C)$_2$] (— —). All spectra were obtained at a molar ratio of 0.2 compound/DNA base-pair and the DNA concentration was 5×10^{-5} M in base-pairs in Pipes 00.

Because of the significant twist of the phenylpyrimidine ring planes of **2b**, it is not possible to form a similar stacked complex of this molecule with a DNA intercalation site. The size and geometry of the overall molecular system of **2b** also do not permit the molecule to fit well into the minor groove of B-form DNA. Quite reasonable models of **2b** in the major groove of DNA can be con-

structed, however, we have no experimental results to support any specific major-groove binding model for **2b** at this time.

4. Discussion

Molecular mechanics calculations indicate that the phenyl-pyrimidine aromatic ring planes of both **1a** and **2a** are twisted with respect to each other by 25–30°. The predicted similarity of twist for these two compounds is strongly supported by NMR studies of the free molecules. The chemical shifts of the phenyl H2′ protons are strongly influenced by the pyrimidine aromatic ring current and are, thus, quite sensitive to the torsional angle between the ring planes. The shifts for the H2′ protons are quite close for **1a** and **2a** (table 2). Crystallographic studies on **1a** have indicated a smaller twist (10–20°) between the two ring planes but this may be partially due to crystal packing forces. Crystal structures for biphenyl, for example, indicate a planar conformation for the two phenyl ring planes in the solid state [36,37].

Molecular mechanics calculations on **1b** and **2b** predict a similar but much larger twist (50–60°) relative to **1a** and **2a**. Again, NMR studies on the free molecules support both of these predictions. First, the phenyl H2′ proton NMR chemical shifts are the same for **1b** and **2b**, indicating a similar torsional angle between the phenyl and pyrimidine ring planes. Second, the H2′ proton signals of **1b** and **2b** are shifted *upfield* by approx. 0.4 ppm relative to the signals in **1a** and **2a**. This indicates that the H2′ protons of **1b** and **2b** are positioned considerably distant from the aromatic ring current deshielding region of the pyrimidine plane as predicted by the calculations.

In spite of the NMR chemical shift similarities of **1a** and **2a**, the absorption spectroscopy maximum for **2a** is shifted 20 nm to longer wavelength relative to **1a**. This, however, is expected due to the much greater conjugative effects of the piperazino nitrogen substituent of **2a** relative to the sulfur substituent of **1a**. In the same manner, the maximum for **2b** is shifted approx. 15 nm to longer wavelength relative to **1b**. The significantly greater twist predicted by molecular mechanics calculations for **1a** and **2a** relative to **1b** and **2b** is strongly supported by the observed spectral peak positions. The greater torsional angles of **1b** and **2b** should reduce conjugation and shift spectra of **1b** and **2b** to lower wavelength relative to **1a** and **2a**. This is observed in both cases (see fig. 5 and ref. 11).

The conformational differences between **1a, 2a** and **1b, 2b** lead to different binding modes for these pairs of compounds with DNA. Both **1a** and **2a** cause similar viscosity increases when added to DNA, and have similar negative reduced dichroism values in their DNA complexes. Although unwinding of closed circular superhelical DNA is generally used as proof for intercalation binding and we have shown that **1a** unwinds DNA, this method is not reliable for organic cations containing unfused ring systems. Dicationic steroids, generally similar in overall shape to **1a, 1b** and **2a, 2b**, unwind DNA but do not intercalate [38]. NMR studies of the protons of ligand provide the only unequivocal indicator of binding mode for these type of compounds. Intercalators stack between DNA base-pairs and the aromatic proton signals of the intercalator shift upfield. In addition, the relative upfield shift of each proton gives a qualitative indication of the extent of stacking of the ligand with base-pairs and can serve as an initial guide in docking experiments in molecular modeling. Ligands which bind in DNA grooves have much smaller induced shifts and these are frequently downfield rather than upfield [1,4,7]. Aromatic protons of both **1a** and **2a** shift significantly upfield on binding to calf thymus DNA and polymers (see table 2, fig. 4 and ref. 11) and are thus clearly established as intercalators. The binding of **1b** to DNA is weaker than that of **1a** and the same is true for the binding of **2b** relative to **2a**. Both **1b** and **2b** cause very small changes in DNA viscosity, have small, positive reduced dichroism values, and very small shifts are induced in their aromatic proton signals on addition of DNA. These results indicate that **1b** and **2b** form weak outside-groove complexes with the DNA double helix. Unwinding studies with **1a, 1b** are in complete support of these conclusions [11].

The different binding modes are also supported by kinetics studies. The dissociation of **1b** and **2b**

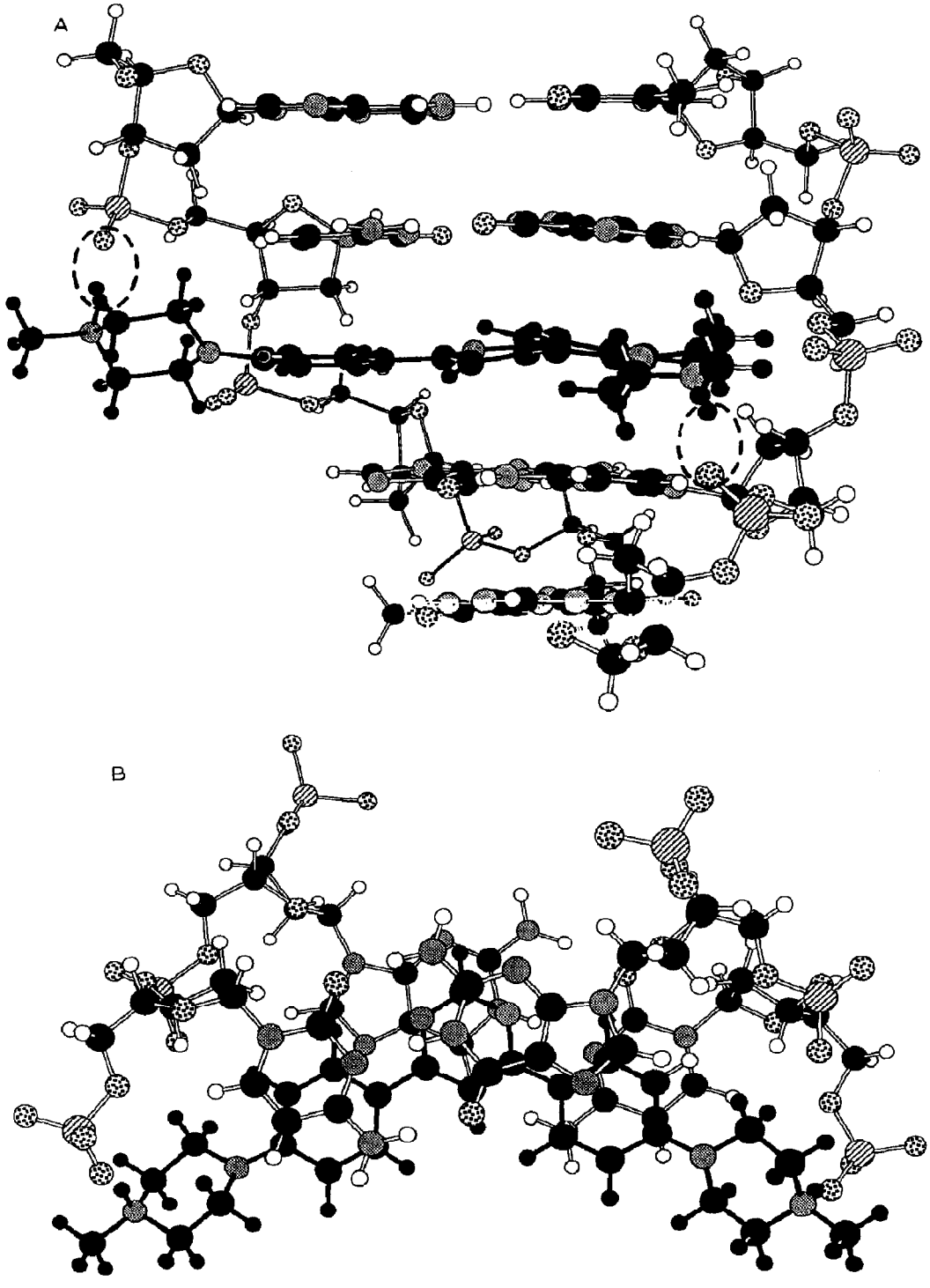
A
B

complexes is too rapid to follow by stopped-flow techniques, but that of **1a** and **2a** can be measured. There are two particularly important observations from the kinetics results. First, dicationic intercalators are predicted to have a slope of approx. 0.6 in log k_d vs. log [Na^+] plots while groove-binding molecules have a slope of 1.6 [28,35]. This significantly different ion release follows from the different mechanism of binding for intercalation and groove complexes [15,28,39]. Intercalators first form an external, ion-condensation type intermediate and insert between DNA base-pairs from this intermediate complex. Groove-binding molecules require less drastic distortions of the DNA double helix and insert into the groove complex in a more concerted fashion [15,28,39]. Both **1a** and **2a** have slopes near 0.6 with calf thymus DNA complexes in support of an intercalation binding mode. Analysis of dissociation of **2a** complexes with poly[$d(A-T)_2$] and poly[$d(G-C)_2$] also yielded slopes of approx. 0.6, indicating a sequence-nonspecific intercalation binding mode for this compound. This is in contrast to other unfused aromatic dications, such as DAPI, which bind strongly in the minor groove at AT sequences but intercalate at GC sequences [15]. Second, significant differences between **1a** and **2a** complexes with DNA are observed in the kinetics experiments. The dissociation rate constant for the **2a**-DNA complex, under a range of ionic strength conditions, is a factor of approx. 10 less than for the **1a** complex (table 4). This result, along with the stronger binding of **2a** to DNA, suggests a more favorable interaction of the rigid piperazino groups of **2a** with DNA than the flexible alkylamine of **1a** in an intercalation complex.

In most experiments with **2a**, similar results are obtained with both poly [$d(A-T)_2$] and poly-[$d(G-C)_2$] and the compound intercalates at both types of sequences based on NMR and kinetics results. The CD spectra of **2a** are, however, quite different with these two polymers (fig. 8). It is known that AT base-pairs have a larger propeller twist than GC base-pairs [5]. This greater propeller twist may allow a greater twist in the phenyl-pyrimidine-phenyl ring system of **1a** and **2a** in an intercalation complex at AT relative to GC sites and, thus, give a greater induced CD ellipticity at AT sites.

Several results suggest that **1a** and **2a** form structurally similar intercalation complexes which cause a distortion of DNA not seen with classical intercalators. The viscosity increases observed with **1a** and **2a** are less than for other intercalators (fig. 3), flow dichroism results are less negative for **1a**- and **2a**-DNA complexes and the aromatic protons of these compounds do not exhibit upfield shifts on addition of DNA as large as those with fused ring intercalators. All these results suggest that **1a** and **2a** do not stack with base-pairs as well as classical fused ring intercalators and may cause slight bending of the DNA helix at the intercalation site.

Although the phenyl-pyrimidine-phenyl aromatic systems of **1a-2a** and **1b-2b** are quite similar in conformation, the piperazino substituents of **2a, 2b** present a larger, more rigid steric constraint to binding than the smaller, more flexible alkylamino cationic side chains of **1a, 1b**. The alkylamino side chains can easily adopt a number of rotationally related conformations which, thus, allow **1a, 1b** more freedom to match the binding site geometry of DNA. It is, thus, surprising that under all observed conditions, **2a** binds to DNA better than **1a** (fig. 7) and dissociates from DNA more slowly than **1a**. Together, these results suggest that the

Fig. 9. (A) A view from one side of the major groove and perpendicular to the helix axis of the central four base-pairs of the energy-minimized complex of **2a** with d(CGTACGTACG). Atoms of **2a** except for nitrogens, which are lightly shaded, are shown in black. In the DNA molecule carbons are darkly shaded, nitrogens lightly shaded, hydrogens unshaded, oxygens dotted, and phosphorous atoms are hatched. Hydrogen bonds between piperazino N-H groups of **2a** and DNA P-O groups are shown by dashed ovals. (B) A view parallel to the helix axis of the central two base-pairs of the **2a**-d(CGTACGTACG) complex. Atom shading is the same as in panel A. The major groove is at the bottom and the minor groove at the top of the plot. Stacking interactions of the **2a** aromatic system with DNA base-pairs can be seen. The DNA chain on the left of the view has the sequence 5′-CG-3′ which gives a CG base-pair on top and a GC base-pair below the intercalated **2a**.

piperazine rings of **2a** are optimally designed for interactions with DNA in a major-groove complex.

Additional information about the **2a** intercalation complexes can be obtained from the molecular modeling/mechanics studies (fig. 9). As predicted from the experimental results, the piperazine rings of **2a** fit snugly into the DNA backbone in the major groove and make good van der Waals contacts (fig. 9A). The piperazine ring is in a chair conformation with equatorial *N*-methyl and axial N-H groups on both rings. The axial N-H protons point directly at phosphate oxygens on the 5′-side of the intercalation site for hydrogen bonding and electrostatic interactions (fig. 9A). The diagonal distance and orientation across the major groove, for P-O groups at both 5′-sides of the intercalation site, are a perfect match for both the distance and orientation of the cationic N-H groups of the piperazine rings of **2a**. The fit of the piperazino groups of **2a** is better than of the alkylamino side chains of **1a** and there are more favorable DNA interactions and possibly less entropy loss on binding of **2a**. It is, thus, clear why **2a** binds more strongly to DNA and dissociates more slowly than **1a**. As with **1a** [11], overlap of the aromatic ring system of **2a** with the DNA base-pairs also provides an important contribution to the complex stability (fig. 9B). The phenyl-pyrimidine torsional angle is 25–30° in the free molecule but is flattened in the complex (fig. 9B). This causes a slight distortion of the pyrimidine and phenyl planes from planarity due to the close contacts of the pyrimidine H-5 with the phenyl H2′ protons. The GC base-pairs on both sides of the bound **2a** molecule are fairly planar and make good van der Waals interactions with the aromatic system of **2a**. The views of the **2a**-DNA complex shown in fig. 9 illustrate why unfused aromatic cations such as **2a** are good bleomycin amplifiers. All of the **2a** molecule is between base-pairs or in the major groove and none of the molecule protrudes into the minor groove. The minor groove is, however, much wider than the normal B-form DNA width because of the separation of base-pairs to form the intercalation site. Slight distortions of the DNA, due to the twisted unfused intercalating ring system, may also facilitate the bleomycin binding and reactive complex formation, and lead to enhanced degradation of the double helix.

Acknowledgments

This work was supported by NSF Grant DMB-8603566, American Cancer Society Grant CH-383, and NIH-NIAID Grant AI-27196. We thank Dr. Clark Still for the MACROMODEL program and Drs. Mike Cory and Robert Jones for assistance and advice in using this program. We thank Dr. Steven Neidle for advice on molecular modeling with DNA in general.

References

1 M. Waring, in: Molecular basis of antibiotic action, eds. F.F. Gale, E. Cundiffe, R.E. Reynolds, M.H. Richmond and M.J. Waring, (Wiley, London, 1981) p. 314.
2 G. Lober, L. Kittler, R. Klarner, Z. Hradecna, V. Kleinwachter, Z. Balacarova, M. Skalka, J. Koudelka, E. Smekal, L. Popa and V. Beensen, Stud. Biophys. 88 (1982) 1.
3 J.W. Lown, Bioactive molecules, vol. 6, Anthracycline and anthracenedione-based anticancer agents (Amsterdam, 1988).
4 S. Neidle and Z. Abraham, CRC Crit. Rev. Biochem. 17 (1984) 73.
5 W. Saenger, Principles of nucleic acid structure (Springer, New York, 1984).
6 C. Zimmer and U. Wahnert, Prog. Biophys. Mol. Biol. 47 (1986) 31.
7 W.D. Wilson and R.L. Jones, Adv. Pharmacol. Chemother. 18 (1981) 117.
8 W.D. Wilson, in: Nucleic acids in chemistry and biology, eds. M. Blackburn and S.M. Gait (IRL Press, Oxford, 1990) ch. 8, in the press.
9 P.B. Dervan, Science 232 (1986) 464.
10 M.L. Kopka, C. Yoon, D. Goodsell, P. Pjura and R.D. Dickerson, Proc. Natl. Acad. Sci. U.S.A. 82 (1985) 1376.
11 W.D. Wilson, L. Strekowski, F.A. Tanious, R.A. Watson, J.L. Mokrosz, A. Strekowska, G.D. Webster and S. Neidle, J. Am. Chem. Soc. 110 (1988) 8292.
12 W.D. Wilson, F.A. Tanious, R.A. Watson, H.J. Barton, A. Strekowska, D.B. Harden and L. Strekowski, Biochemistry 28 (1989) 1984.
13 L. Strekowski, S. Chandrasekaran, Y.H. Wang, W.D. Edwards and W.D. Wilson J. Med. Chem. 29 (1986) 1311.
14 L. Strekowski, W.D. Wilson, J.L. Mokrosz, A. Strekowska, A.E. Koziol and G.J. Palenik, Anti-Cancer Drug Design 2 (1988) 387.
15 W.D. Wilson, F.A. Tanious, H.J. Barton, R.L. Jones, L. Strekowski and D.W. Boykin, J. Am. Chem. Soc. 111 (1989) 5008.

16 J. Kapuscinski and W. Szer, Nucleic Acids Res. 6 (1979) 3519.
17 G. Manzini, M.L. Barcellona, M. Avitabile and F. Quadrifoglio, Nucleic Acids Res. 11 (1983) 8861.
18 Z. Balcarova, V. Kleinwachter, G. Lober, G. Luck, C. Zimmer and R. Klarner, Biophys. Chem. 9 (1979) 121.
19 L. Strekowski, J.L. Mokrosz, F.A. Tanious, R.A. Watson, D. Harden, M. Mokrosz, W.D. Edwards and W.D. Wilson, J. Med. Chem. 31 (1988) 1231.
20 D.J. Brown and G.W. Grigg, Med. Res. Rev. 2 (1982) 193.
21 J. Stubbe and J.W. Kozarich, Chem. Rev. 87 (1987) 1107.
22 S.M. Hecht, Acc. Chem. Res. 19 (1986) 383.
23 P.E. Pjura, K. Grzeskowiak and R.E. Dikerson, J. Mol. Biol. 197 (1987) 257.
24 M.-K. Teng, N. Usman, C.A. Fredrick and A.H.-J. Wang, Nucleic Acids Res. 16 (1988) 2671.
25 I. Husain and S.K. Agarwal, Indian J. Chem. 13 (1975) 1238.
26 J. L. Hartwell, Org. Synth. Coll. 3 (1955) 185.
27 D.B. Harden, M.J. Mokrosz and L. Strekowski, J. Org. Chem. 53 (1988) 4137.
28 W.D. Wilson, C.R. Krishnamoorthy, Y.H. Wang and J.C. Smith, Biopolymers 24 (1985) 1941.
29 W.D. Wilson, Y.-H. Wang, S. Kusuma, S. Chandrasekaran, N.C. Yang and D.W. Boykin, J. Am. Chem. Soc. 107 (1985) 4989.
30 R.L. Jones, A.C. Lanier, R.A. Keel and W.D. Wilson, Nucleic Acids Res. 8 (1980) 1613.
31 J.D. McGhee and P.H. von Hippel, J. Mol. Biol. 86 (1974) 469.
32 D.L. Banville, L.G. Marzilli and W.D. Wilson, Inorg. Chem. 24 (1985) 2481.
33 C.R. Krishnamoorthy, S.F. Yen, J.C. Smith, W. Lown and W.D. Wilson, Biochemistry 25 (1986) 5933.
34 S. Chandrasekaran, S. Kusuma, D.W. Boykin and W.D. Wilson, Magn. Reson. Chem. 24 (1986) 630.
35 M.T. Record, Jr., C.F. Anderson and T.M. Lohman, Q. Rev. Biophys. 11 (1978) 103.
36 A. Hargraves and S. Hasan-Rizvi, Acta Crystallogr. 15 (1962) 365.
37 J. Troller, Acta Crystallogr. 14 (1961) 1135.
38 M.J. Waring and S.M. Henley, Nucleic Acids Res. 2 (1975) 567.
39 J.A. Strickland, L.G. Marzilli, K.M. Gay and W.D. Wilson, Biochemistry 27 (1988) 8870.